

Growth and Characterizations of Rhenium Disulfide (ReS₂) Single Crystals

Atriy Ghetiya,* Sunil H. Chaki,* Ankurkumar J. Khimani, Anilkumar B. Hirpara, Rohitkumar M. Kannaujiya, Shivam Patel, and Milind P. Deshpande

Rhenium disulfide (ReS₂) single crystals are grown by chemical vapor transport technique. Powder X-ray diffraction analysis of the single crystals shows them to possess ReS₂ phase with triclinic unit cell structure. Energy dispersive analysis of X-rays shows the crystals to be slightly rich in sulfur and deficient in rhenium. The optical bandgap obtained of the as-grown single crystals is 1.35 eV. The surface morphology study done by scanning electron microscopy shows that the crystal surface to be flat with layer edges, such observation states that the growth mechanism of crystal have happened by mechanism of sheet spreading. The transmission and diffraction mode electron microscopy shows the single crystals to be layered and crystalline, respectively. The Raman peaks are well assigned to the ReS₂. Thermogravimetric and differential thermogravimetric analysis shows the single crystals to disintegrate by two steps. The differential thermal analysis shows that the ReS₂ possesses initial endothermic followed by exothermic nature for fast heating rates. In case of a slow heating rate of 10 K min⁻¹, other than endothermic followed by exothermic, the end temperature range shows endothermic nature. The kinetic parameters determined by Kissinger relation shows the single-crystal samples to disintegrate at a higher temperature range.

between the atoms is of strong covalent type and between the interlayers is of very weak van der Waals type.^[8] Thus, the TMDCs can be exfoliated from multilayer 3D to monolayer 2D, thus providing immense opportunity to be of worth in present day device miniaturization.^[9] The 3D bulk TMDCs exhibit indirect optical bandgap which transforms to direct optical bandgap when trimmed down to 2D monolayer.^[10] The varied TMDC optical bandgap values fall within the range of solar spectrum of 1–2.5 eV as well as their electrical transport properties are in complement with high-quality semiconductor properties.^[3] These favorable basic optical and electrical properties make TMDCs a potential material for optoelectronic devices. The 2D monolayer TMDCs have isotropic transport properties, and due to presence of weak van der Waals bonding between stacked layers, the 3D TMDCs possess anisotropic properties.

1. Introduction

The transition metal dichalcogenides in short expressed as TMDCs are compound semiconductors with advanced properties, and have thus found to surmount the erstwhile silicon technology.^[1–5] The TMDCs possess lamellar layered structure with each layer formed of a combination of transition metals and chalcogens with formula MX₂ (M: transition metals; X: chalcogens) arranged to form a thin layer. The layers get stacked one on another to form the bulk. A single layer of TMDCs is formed of metal ions sandwiched between two chalcogens.^[6,7] The intralayer bonding

The transition from indirect to direct optical bandgap happens when the dimension of a sample decreases from 3-dimensions to 2-dimensions in the case of TMDCs materials. The potential basic properties of TMDCs and their swift variation during trimming from multi to monodimension attracted researchers to perform studies on them in this age of compactness and efficiency. The most studied TMDCs are the elemental combination formed of group elements from IVB (Ti, Zr), VB (V, Nb, Ta), VIB (Cr, Mo, W) metal atoms and group VIA (S, Se, Te) chalcogen atoms. Recently, other than the conventional TMDCs, a TMDC formed of group VIIB element Re with chalcogens has received much interest. This is due to its anisotropic properties even in monolayer, the converse of other TMDCs,^[11] whereas the optical bandgap variation from indirect to direct with decrease in layers observed in other TMDCs is not observed in Re chalcogenides. The Re chalcogenide shows a direct optical bandgap in all dimensions. These complementary properties of Re chalcogenides compared to other TMDCs have attracted many researchers to study the compounds in different forms ranging from nano to thin films and crystals.^[12–14] The authors got interested due to these properties of the Re chalcogenides and did comprehensive study on ReS₂ in its single-crystal form.

ReS₂ does not possess conventional TMDC 2H structure but possesses a twisted 1T phase.^[15] The lesser symmetry causes anisotropy in electronic^[16] and optical properties^[17,18] in the monolayer dimension. The experimental study of ReS₂ optical

A. Ghetiya, Dr. S. H. Chaki, Dr. A. J. Khimani, A. B. Hirpara, R. M. Kannaujiya, Dr. S. Patel, Dr. M. P. Deshpande
P. G. Department of Physics
Sardar Patel University
Vallabh Vidyanagar, Gujarat 388120, India
E-mail: atriyghetiya@gmail.com; sunilchaki@yahoo.co.in
Dr. S. H. Chaki
Department of Applied and Interdisciplinary Sciences
Sardar Patel University
Vallabh Vidyanagar, Gujarat 388120, India

 The ORCID identification number(s) for the author(s) of this article can be found under <https://doi.org/10.1002/pssa.202000687>.

DOI: 10.1002/pssa.202000687

absorbance and theoretical study by density functional theory (DFT) showed it to possess a direct optical bandgap in the range 1.3–1.6 eV for both the bulk and monolayer.^[19–22] Thus, the optical bandgap of ReS₂ is isotropic in nature. In contrast, the transport properties are anisotropic in nature; they vary with the dimensions of the layers.^[16] The isotropic optical bandgap of ReS₂ matches with the solar range. Thus the isotropic bandgap and the anisotropic transport properties make ReS₂ a potential applicant in photocatalysis, solar cells, photodetectors, supercapacitor, etc.^[20] The other applications of ReS₂ are in nitrogen reduction reaction and hydrogen evolution reaction.^[14,23] These applications arise due to the weak interlayer coupling in ReS₂, thus proving it to be a lead material for future green chemistry at ambient condition.^[14,23] The varied electrical transport nature of ReS₂ makes it interesting for a variety of energy conversion and storage base applications.^[24,25] In this study the authors grew single crystals of ReS₂ by chemical vapor transport (CVT) technique in a closed tube schematic. The grown single crystals were completely characterized for their varied basic properties before performing thorough thermal study.

2. Experimental Section

The ReS₂ single crystals were grown by CVT using iodine as the transporting agent. Rhenium metal powder (SRL, India, purity 99.9999%) and sulfur powder (Alfa Aesar, USA, purity 99.99%) were loaded in stoichiometric proportion in an HCl, HF washed and double distilled water rinsed fully dried quartz ampoule. Along with precursor elements, iodine was also put into the ampoule as a transporting agent. The total weight of the stoichiometric elemental composition loaded into the quartz ampoule was not more than 8 gm. The transporting agent iodine amount was taken at the rate of 4 mg cc⁻¹ of ampoule dimension. The quartz ampoule dimension was 2 cm (I.D.) × 20 cm (length). The precursor element-loaded quartz ampoule was evacuated to ≈10⁻⁵ torr and vacuum sealed. The individual elements were well mixed by vigorous physical shaking of the ampoule. The complete elemental mix is kept at one end of the ampoule known as the charge zone and the empty end of the ampoule was the growth zone. The vacuum-sealed quartz ampoule having the elemental mix at the charge zone end and the other growth zone end empty was placed in a horizontal dual-zone cylindrical furnace. The temperature of the furnace was slowly raised at a rate of 16 K min⁻¹ such that the elemental mix-loaded quartz ampoule's charge zone was at 1093 K and growth zone was at 1043 K. The ampoule was maintained at these intermediate temperatures for 50 h. This process of maintaining the elemental mixture-filled ampoule for a finite time period at intermediate temperature was to allow the precursor elements to react with each other to form the ReS₂ compound. Next the ampoule temperature was further raised to single-crystal growth temperatures such that the charge zone was at 1393 K and the growth zone was at 1343 K. The ampoule was kept in this growth temperature range for 120 h. On completion of the growth run, the furnace temperature was slowly cooled down to ambient condition at slow cooling rate of 30 K min⁻¹. Slow cooling was preferred to avoid thermal cracks in the grown single crystals. After the ampoule was cooled to ambient

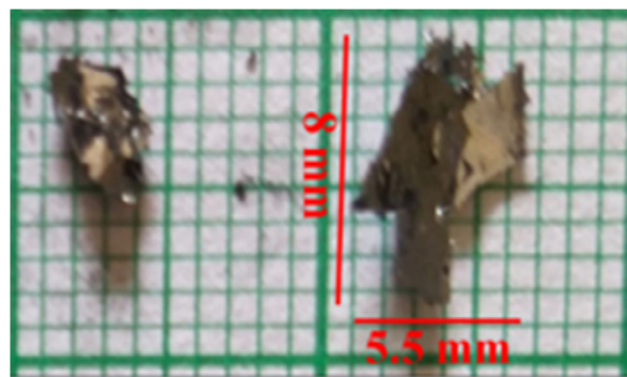


Figure 1. Photograph of CVT as-grown ReS₂ single crystals.

condition, it was removed from the furnace muffle and carefully broken at the growth zone region to retrieve the grown single crystals. A photograph of average large size CVT as-grown ReS₂ single crystals is shown in **Figure 1**. The ReS₂ single crystals were shining brownish black in color with average large size dimensions of 8 mm × 5.5 mm × 2 mm.

3. Characterization

The CVT as-grown ReS₂ single crystals were fully characterized for crystal structure, stoichiometry, morphology, etc. before performing in-depth thermal analysis. A Philips X'PERT MPD powder X-ray diffractometer was used to analyze the phase and unit cell structure of the sample. The stoichiometry of the single-crystal sample was determined by dispersive energy analysis of X-rays (EDAX) technique attached to a NOVA-450 electron microscope. The optical absorption study was conducted with the help of a double beam double monochromator ratio recording, Perkin Elmer Lambda-19 UV-vis-NIR spectrophotometer. The electron microscope used for EDAX analysis in scanning (SEM) mode was used to study the surface morphology of the as-grown single crystal sample. A JEOL JEM-2100 HR electron microscope was used in high-resolution transmission (HRTEM) and diffraction (SAED) modes to characterize the as-grown single-crystal sample. The Raman spectroscopy on the as-grown ReS₂ single crystals was done by a micro-Raman model STR 500. The thermocurves of the single-crystal samples were recorded using a Seiko SII-EXSTAR TG/ DTA-7200 thermal analyzer.

4. Results and Discussion

4.1. Structure

The X-ray diffraction (XRD) of the as-grown ReS₂ single crystal is shown in **Figure 2**. The analysis of the XRD pattern was done by PowderX software. All the peaks are indexed as that of ReS₂ possessing triclinic unit cell structure having lattice parameters $a = 0.641$ nm, $b = 0.634$ nm, and $c = 0.645$ nm and angles $\alpha = 91.60^\circ$, $\beta = 105.04^\circ$, and $\gamma = 118.97^\circ$. The obtained lattice parameters and angles matched with standard reported data^[26,27] and JCPDS File No. 052-0818. The XRD shows the (001) plane to be the most prominent compared to other observed planes. This

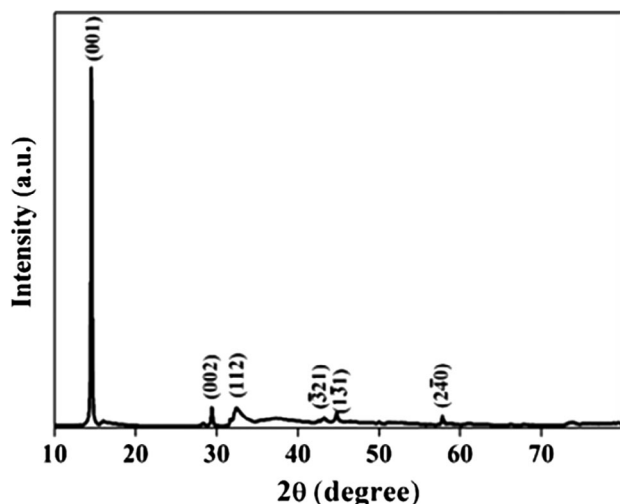


Figure 2. The XRD of as-grown ReS₂ single crystals.

confirms that the growth of the ReS₂ single crystal have happen along the direction of (001) plane. The unit cell volume determined from the observed lattice parameters is 54.75 Å³. The determined unit cell volume matches the reported unit cell volume of 54.75 Å³.^[28]

4.2. Elemental Composition

The EDAX spectrum of the CVT as-grown ReS₂ single crystal is shown in **Figure 3**.

The spectrum shows the presence of only two peaks corresponding to Re and S, showing no impurity in the as-grown single crystals. The observed EDAX data along with standard data are tabulated in **Table 1**.

Comparison of both the observed and standard data shows the as-grown single crystals to be of ReS₂ stoichiometry. The as-grown single crystals are slightly Re deficient and S rich.

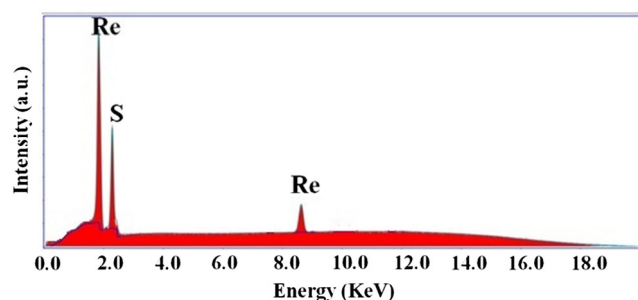


Figure 3. The EDAX spectrum of ReS₂ single crystals.

Table 1. The EDAX data of CVT as-grown ReS₂ single crystals.

Element	Weight%		Atomic%	
	Observed	Standard	Observed	Standard
Re	74.27	74.38	65.84	66.66
S	25.73	25.62	34.16	33.33

4.3. Optical Properties

The recorded optical absorption spectrum in the wavelength range of 300–1500 nm for the as-grown ReS₂ single crystals is shown in **Figure 4a**. The spectrum showed that the as-grown ReS₂ single crystals have absorbance in the wavelength range of ≈560–720 nm. The optical bandgap is determined using the relation $(\alpha h\nu)^n = A(h\nu - E_g)$, where n represents the transitions, A is the optical transition-dependent constant, E_g is the optical energy bandgap, ν is the frequency of the incident beam, h is Planck's constant, and α is the absorption coefficient. The value of the optical energy bandgap E_g obtained from the graph of $(\alpha h\nu)^2$ versus $h\nu$, **Figure 4b**, taking the intercept on the $h\nu$ axis came out to be 1.35 eV. This direct optical bandgap value lies within the reported value of 1.3–1.5 eV.^[19–22] The observation shows that the obtained direct optical bandgap value is in good agreement with the reported value.

4.4. Field Emission Scanning Electron Microscopy (FESEM)

The common features observed on the as-grown CVT ReS₂ single-crystal surfaces under FESEM are shown in **Figure 5a,b**. The photographs of fresh single crystals were taken just after retrieval from the ampoule after the crystal growth run. The analysis of the photographs (**Figure 5a**) clearly shows the crystal surface to be flat. A few flakes of the crystals are observed on the flat surface (**Figure 5b**). Other than this, iodine patches are also observed on the surface. The iodine patches are formed from the cooling of the transporting agent on the smooth crystal surface during crystal growth. The flat surfaces of the crystal faces confirm the crystal growth to have happened by the sheet-spreading mechanism. During crystal growth the charge powder evaporates from the high-temperature end of the charge zone to settle to the lower temperature growth zone end to form crystals at the nucleation sites. The transportation is done by the transporting agent iodine. The transported charge powder grows to a crystal by the sheet spread mechanism, thus forming a flat surface. No other dislocations or defects are observed on the surfaces, showing the present growth condition to be optimum for the growth of ReS₂ single crystals by the sheet spread mechanism.

4.5. High-Resolution Transmission Electron Microscopy (HRTEM)

The recorded HRTEM image and the SAED pattern of the CVT as-grown ReS₂ single crystals is shown in **Figure 6a,b**, respectively. The samples for the electron transmission and diffraction analysis were prepared by exfoliating the ReS₂ single crystals. The as-grown single crystals were dispersed in *N*-methyl-2-pyrrolidone (NMP) and ultrasonicated for 3 h. After 3 h ultrasonication a drop was taken on a carbon film present on a copper grid sample holder for HRTEM analysis. The excess NMP was absorbed by filter paper and allowed to dry in the open. The HRTEM image of the taken ReS₂ exfoliated sample, shown in **Figure 6a**, clearly shows overlap of multiple layers of the ReS₂ sample. The overlap of multiple layers shows the sheet spread mechanism to be the means of crystal growth. This result of HRTEM substantiates the FESEM observation. The SAED

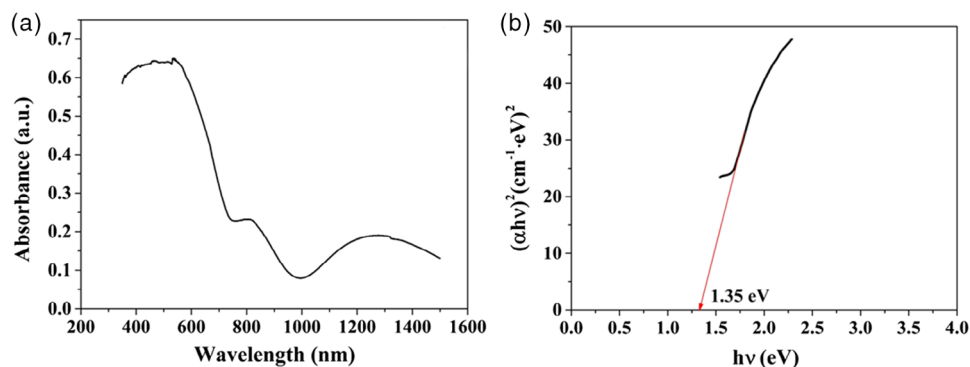


Figure 4. The a) absorbance spectrum and b) plot of $(\alpha hv)^2$ versus $h\nu$ of ReS_2 single crystals.

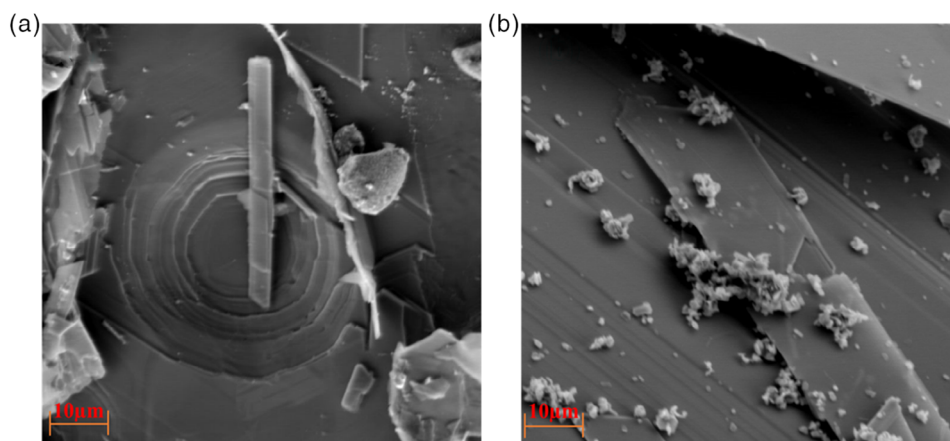


Figure 5. FESEM images of CVT as-grown ReS_2 single crystals at two different magnifications.

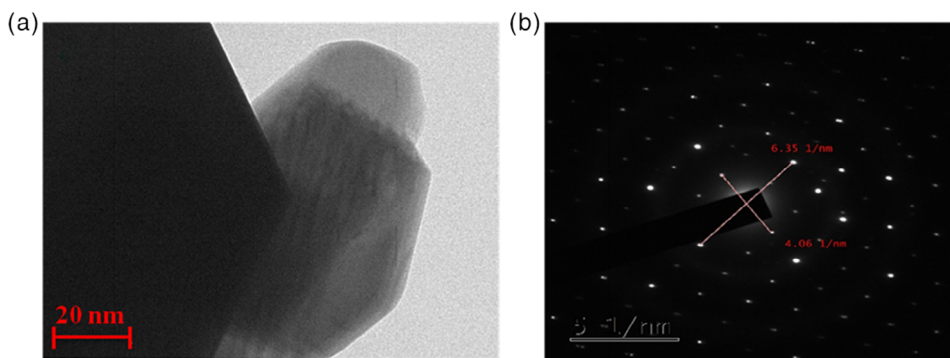


Figure 6. a) HRTEM image and b) SAED pattern of CVT as-grown ReS_2 single crystals.

image, shown in Figure 6b, shows the presence of a well-organized spot pattern confirming the sample to be single crystal.

4.6. Raman Spectroscopy

The recorded Raman spectrum on CVT as-grown ReS_2 single crystal is shown in Figure 7.

All the observed Raman peaks along with frequency positions are tabulated in Table 2. The reported standard

Raman data are also given in the table to compare with the observed data.^[29]

The observed initial Raman peaks lying in the range 145.1 and 285.6 cm^{-1} are the primary ones which match with the standard reported peaks of exfoliated ReS_2 .^[30,31] Minor disparities in the peak positions are observed; these arise due to the different crystallite sizes and plane orientations of the present crystals. Also, the variation arises due to different growth conditions in this case. The peaks lying in the higher wavenumber region $312.8\text{--}420.8 \text{ cm}^{-1}$ are comparatively weak. They match

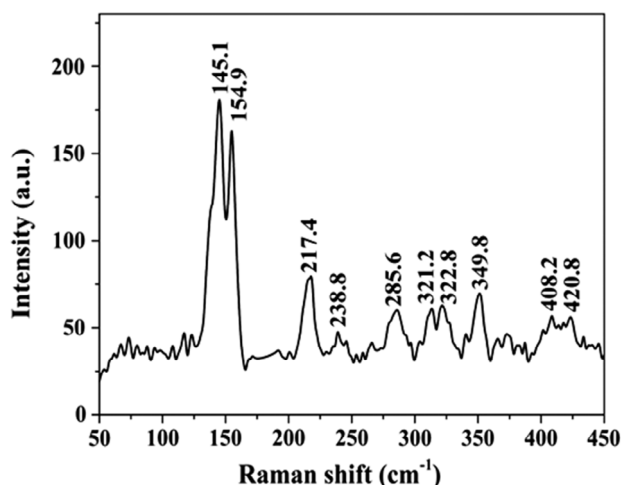


Figure 7. The Raman spectrum of CVT as-grown ReS_2 single crystals.

Table 2. The Raman data of as-grown ReS_2 single crystals along with standard data.

Observed Raman frequency [cm^{-1}]	Standard Raman frequency [cm^{-1}]	Symmetry mode	Origin of phonon mode
145.1	145.9	A_g	Out-of-plane vibrations of Re atoms
154.9	153.1	E_g	In-plane vibrations of Re atoms
217.4	217.2	E_g	In-plane vibrations of Re atoms
238.8	237.1	E_g	In-plane vibrations of Re atoms
285.6	284.2	C_p	In-plane and out-of-plane vibration of Re and S atoms
312.8	311.0	E_g	In-plane and out-of-plane vibration of Re and S atoms
322.2	324.9	C_p	In-plane and out-of-plane vibration of S atoms
349.8	348.8	C_p	In-plane and out-of-plane vibration of S atoms
408.2	407.3	C_p	In-plane and out-of-plane vibration of S atoms
420.8	418.7	A_g	Out-of-plane vibrations of S atoms

well with the reported peaks^[31,32] and are the second order Raman modes. The symmetry and phonon modes assigned to the observed Raman peak and reported data are also tabulated in Table 2.

4.7. Thermal Analysis

The recorded thermogravimetric (TG), differential thermogravimetric (DTG), and differential thermal analysis (DTA) curves of CVT as-grown ReS_2 single crystals are shown in Figure 8a–c. The thermocurves are recorded in the temperature range of ambient and 1233 K in inert nitrogen (N_2) atmosphere. The curves are recorded simultaneously for three heating rates of 10, 15, and 20 K min^{-1} . The starting weights of single-crystal samples taken for all thermal analyses are between 11 and 13 mg.

The analysis of TG curves (Figure 8a) shows the single-crystal samples to have minor weight loss in the initial temperature range followed by continuous weight loss till the measured temperature of 1233 K. The nature of the curves is near-similar for all three heating rates. The corresponding DTG curves display two peaks, showing that the single-crystal samples decompose in two steps. The temperature ranges for both the regions having minor and major weight loss in percentage data are tabulated in Table 3. The temperature range of the TGs is determined from the DTG peaks' positions. The end point of the derivative of the weight loss is considered to be the finish point of the first temperature range, 509 K.

The thermal data in Table 3 show that the ReS_2 single crystals had negligible weight loss in the temperature range of step I, ambient to ≈ 509 K for all three heating rates. The weight losses for the three heating rates are below 1%. The minor initial weight losses are due to loss of moisture from the hydrous samples as well as removal of lightly attached molecules from the samples. The EDAX showed the single crystals to be slightly sulfur rich, which gets removed in the initial temperature rise. The cause is that the vaporization of the sulfur element is far below that of the rhenium element. This observation shows the CVT as-grown ReS_2 single crystals to be stable in the temperature range of ambient to 509 K.

In the temperature range of step II, from 510 to 1233 K the samples showed major weight loss, showing the disintegration of the single-crystal samples. Detailed observation of the curves, as shown in Figure 8a, shows that as the heating rate increases the weight loss increases. The percentage weight loss in case of a heating rate of 10 K min^{-1} is $\approx 18.56\%$, whereas it increases to 35.02% in case of 15 K min^{-1} heating rate and for the heating rate of 20 K min^{-1} the weight loss is nearly 70.31%. The observation affirms that when the heating rate increases, the sample decomposition temperature shifts toward lower values, meaning

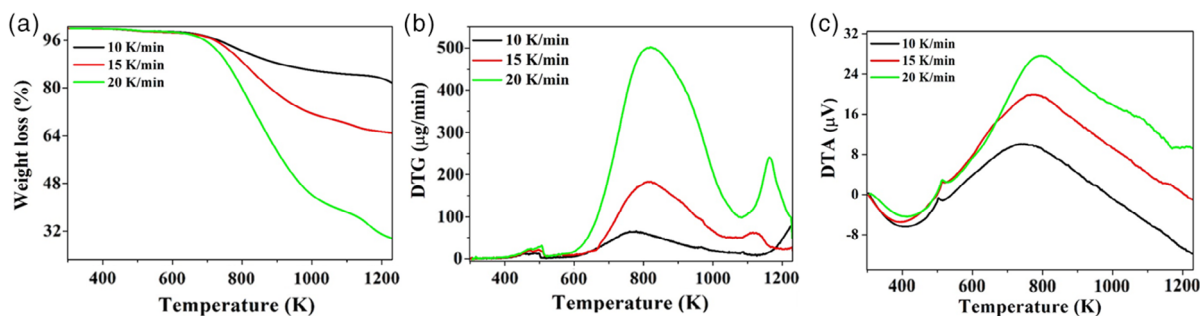


Figure 8. The a) TG, b) DTG, and c) DTA curves of CVT as-grown ReS_2 single crystals.

Table 3. The thermal data of CVT as-grown ReS₂ single crystals.

Heating rates [K min ⁻¹]	Weight loss [%]		Total weight loss [%]	DTG peak position T _m [K]	
	Temperature range			1st peak	2nd peak
	Step I	Step II	303–1233 K		
	303–509 K	510–1233 K			
10	0.85	17.71	18.56	492.01	797.54
15	0.94	34.08	35.02	493.89	800.81
20	0.84	69.47	70.31	497.32	803.04

that at a higher heating rate, the sample gets heated to a temperature in a short span and thus the decomposition temperature shifts to a lower value. The impetuous temperature rise due to high heating rates enhances the sample decomposition, resulting in high weight loss.^[33] Thus, with increased heating rates the weight loss increases.

The corresponding DTG curves, displayed in Figure 8b, clearly show the presence of two peaks. This further substantiates the observation of TG curves stating two-step decomposition of the CVT as-grown ReS₂ single crystals. The DTG peak positions T_m are tabulated in Table 3. The T_m values for both the peaks clearly shows that as the heating rate increases the magnitude value increases. This happens due to the prevalence of heat transfer constraints^[34,35] at high heating rates. The simultaneously recorded DTA curves show that for heating rates of 15 and 20 K min⁻¹ (Figure 8c) there is an initial endothermic nature followed by exothermic nature. But for the heating rate of 10 K min⁻¹ (Figure 8c) there is an initial endothermic nature followed by exothermic and at last endothermic. The initial endothermic nature for all three heating rates are due to vaporization of the moisture from the hydrous sample as well as release of lightly attached molecules on the sample surfaces. In the present sample the lightly attached molecules are the slightly excess sulfur as confirmed from the EDAX data. The outgoing moisture as well as the lightly attached molecules takes away the heat, leading to the endothermic nature. The loss of moisture, as well as lightly attached molecules, is confirmed by the minor weight loss observed in the same temperature range, step I, of TG curves. The exothermic nature after the step I temperature range shows disintegration of the ReS₂ sample with temperature rise. The sample disintegration releases energy in the form of heat, showing the exothermic nature. In the case of the 10 K min⁻¹ heating rate, an endothermic nature is observed at the end range of the analyzed temperature, 980 and 1233 K. This appears due to slow heating. At a slow heating rate the applied heat gets fully dissipated amongst the sample, leading to complete disintegration of the sample before melting. In case of fast heating rates of 15 and 20 K min⁻¹ the endothermic nature gets shifted to a high-temperature range due to heat transfer constraints.^[34,35]

In all the DTA curves a small kink is observed at around the temperature of 500 K. The kink is seen to shift to higher temperature for faster heating rates. The experimental limitations constrain the understanding of the kink in the DTA curves.

4.8. Kissinger Relation

The important thermodynamic parameters of the CVT as-grown ReS₂ single crystals are determined using the Kissinger relation. In these calculations the thermal parameters obtained from the DTG curves are used. The mathematical expression of the Kissinger relation is as shown.^[29]

$$\ln \frac{\beta}{T_m^2} = \ln \frac{AR}{E_a} + \ln \left[\frac{d\{f(\alpha)\}}{d\alpha} \right] - \frac{E_a}{RT_m} \quad (1)$$

where α is the fraction of weight loss and $f(\alpha)$ is the function that relies on the value of α . This equation is strictly constrained to a first order reaction value as per the kinetic model, i.e., $d\{f(\alpha)\}/d\alpha = -1$, and so its value should be independent of the heating rate. Otherwise, the value of the initial term on the right-hand side of Equation (1) would be changed, and the activation energy value obtained consist of some error, and the Kissinger plot would be out of its linearity.^[29] Therefore, the $d\{f(\alpha)\}/d\alpha$ term is eliminated and further simplification is deduced as^[31]

$$\ln \frac{\beta}{T_m^2} = \ln \frac{AR}{E_a} - \frac{E_a}{RT_m} \quad (2)$$

Here, β denotes the heating rate, T_m is the DTG peak positions, and R is the gas constant. The Arrhenius plot between $\ln \frac{\beta}{T_m^2}$ and $\frac{1}{T_m}$ for CVT as-grown ReS₂ single crystals is shown in Figure 9a,b. The two curves are for two peaks.

The thermodynamic parameters activation energy (E_a), activation enthalpy difference (ΔH), activation entropy difference (ΔS), and Gibb's free energy change (ΔG) for CVT as-grown ReS₂ single crystals are calculated from the slopes and intercepts obtained from the Kissinger plots, (Figure 9a,b). The equations used for the calculations of the thermodynamic parameters are as follows

$$\Delta H = E_a - RT_m \quad (3)$$

$$\Delta S = 2.303R \log \left(\frac{Ah}{kT_m} \right) \quad (4)$$

$$\Delta G = \Delta H - T\Delta S \quad (5)$$

The determined kinetic parameters of the CVT as-grown ReS₂ single-crystal samples are tabulated in Table 4.

The thermal activation energy E_a values obtained for the CVT as-grown ReS₂ single crystals show that the magnitude value of E_a is large for step II compared to step I. The reason is the weight loss is highest in the temperature range of step II. This is due to disintegration of the single-crystal samples at high temperature. The large value of E_a shows the sample disintegration due to high temperature. The determined Arrhenius constant A values are large in step II compared to step I, further supporting the observation of the large E_a value in step II.

The determined ΔS values show that it is negative in step I and step II. The negative ΔS value in step I states ordering to happen with rise in temperature. The step I temperature between ambient and 509 K removes moisture as well as the lightly attached molecules along with the minor defects, dislocations, stress, etc. The negative value of ΔS substantiate that the

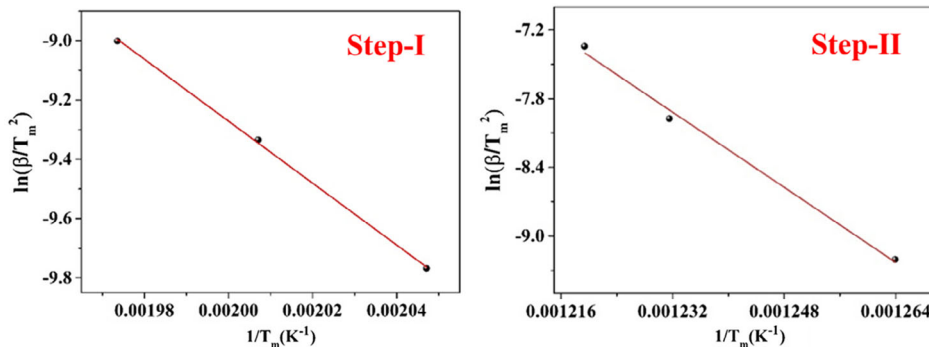


Figure 9. The Kissinger plots of as-grown ReS₂ single crystals.

Table 4. The thermodynamic parameters of CVT as-grown ReS₂ single crystal.

DTG Peak	E_a [J mole ⁻¹]	A [min ⁻¹]	ΔS [J · K ⁻¹ mole ⁻¹]	ΔH [J mole ⁻¹]	ΔG [kJ mole ⁻¹]
Step I	5379.08	2.28	-557.95	821.60	500.008
Step II	20492.65	23.67	-522.37	13837.23	481.188

ordering occurs in the crystal by removal of defects, dislocations, stress, etc. The removal of moisture and lightly attached molecules gives negligible weight loss in step I. However, in step II, the material gets ordered before commencing of structure degradation. The determined ΔH values are positive for both the steps, showing absorption of heat. The ΔH value is more in step II compared to step I, thus showing absorption of more heat in step II. The large heat absorption leads to disintegration of ReS₂ single crystals. The disintegration is corroborated by the maximum weight loss in the temperature range of step II. Step I also has ΔH positive but the magnitude value is small, showing no sample disintegration. The weight loss in step I is also small and is due to moisture evaporation and loss of lightly attached molecules. The ΔG values are positive for both the steps. The positive ΔG values show the process of disintegration to be nonspontaneous. All the parameters calculated earlier are representing DTG peak positions shown in Table 3. The overall inference drawn from the determined thermodynamic parameters are the CVT as-grown ReS₂ single crystals are stable in the initial temperature range of ambient to 509 K. Above this temperature range, 510–1233 K, the samples disintegrate and lead to weight loss.

5. Conclusion

Single crystals of ReS₂ are successfully grown by CVT technique using iodine as the transporting agent. The powder XRD of as-grown crystals showed them to be single-phase ReS₂ having triclinic unit cell structure in good match with the reported data. The EDAX of the crystals showed them to be free of any impurity and slightly rhenium deficient and sulfur rich. The optical analysis in the wavelength range of 300 and 1500 nm showed that the as-grown ReS₂ single crystals possess a direct optical bandgap of

1.35 eV. The microstructure study by FESEM showed flat surfaces having layer edges confirming crystal growth by the sheet spread mechanism. The layered nature of the as-grown crystals is confirmed by HRTEM analysis and the spot SAED pattern confirmed the crystalline character. The Raman spectroscopy of the crystals showed all the peaks are of ReS₂ only. The TG analysis showed the CVT as-grown ReS₂ single-crystal samples to disintegrate by two steps. The two-step disintegration is supported by the presence of two peaks in the corresponding DTG curves. The corresponding DTA showed an initial endothermic and later exothermic nature for faster heating rates of 15 and 20 K min⁻¹. The slow heating rate of 10 K min⁻¹ showed the initial endothermic followed by exothermic and at later high temperature an endothermic nature. The thermodynamic parameters determined using Kissinger relations showed the thermal activation energy value to be high in the high-temperature range compared to the low-temperature range. This indicates decomposition of the sample at high temperature. The entropy change of the sample showed negative value in both steps. The negative value in the initial temperature range shows ordering to occur with temperature rise. The enthalpy change is positive in both the steps, indicating heat absorption by the sample. The Gibbs free energy change values are positive for both the steps, showing prompt nonspontaneous absorption of heat as the temperature rises. The thermodynamic parameters showed the single-crystal samples disintegrate at high temperature, leading to weight loss being observed in the TG curves. This study showed good-quality single crystals with least defects as observed from the FESEM can be grown by CVT. The direct optical bandgap of the as-grown CVT ReS₂ lying in the visible range with good thermal stability upto ≈509 K makes it an impending aspirant for optoelectric applications.

Acknowledgements

A.G. is thankful to the Scheme of Developing High Quality Research (SHODH) by KCG (Knowledge Consortium of Gujarat)—Government of Gujarat for providing financial support in research and analysis. A.B.H. is thankful to the Department of Science and Technology (DST), Technology Bhawan, New Mehrauli Road, New Delhi-110016, for the award of the INSPIRE Fellowship (IF180246) to conduct this research work. All the authors are thankful to the Sophisticated Instrumentation Centre for Applied Research & Testing (SICART), Vallabh Vidyanagar, Gujarat, India, for XRD, EDAX, FESEM, UV–vis–NIR spectroscopy analysis, and DST- SAIF, Cochin, for HRTEM of the samples.

Conflict of Interest

The authors declare no conflict of interest.

Data Availability Statement

Research data are not shared.

Keywords

characterization, chemical vapor transport, ReS₂, single crystals, thermal analysis

Received: November 3, 2020

Revised: March 9, 2021

Published online:

-
- [1] S. Yu, X. Wu, Y. Wang, X. Guo, L. Tong, *Adv. Mater.* **2017**, *29*, 1606128.
- [2] H. Taghinejad, A. Eftekhar, A. Adibi, *Opt. Mater. Express.* **2019**, *9*, 1590.
- [3] M. Taghinejad, Z. Xu, H. Wang, H. Taghinejad, K. T. Lee, S. P. Rodrigues, A. Adibi, X. Qian, T. Lian, W. Cai, *Small* **2020**, *16*, 1.
- [4] S. H. Chaki, G. K. Solanki, A. J. Patel, S. G. Patel, *High Press. Res.* **2008**, *28*, 133.
- [5] S. Chaki, A. Agarwal, *Synth. React. Inorganic, Met. Nano-Metal Chem.* **2008**, *38*, 267.
- [6] C. W. Monolayers, *Large-Area Synthesis of Highly*, American Chemical Society, Taipei, Taiwan **2013**.
- [7] J. P. Tailor, D. S. Trivedi, S. H. Chaki, M. D. Chaudhary, M. P. Deshpande, *Mater. Sci. Semicond. Process.* **2017**, *61*, 11.
- [8] W. S. Yun, S. W. Han, S. C. Hong, I. G. Kim, J. D. Lee, *Phys. Rev. B – Condens. Matter Mater. Phys.* **2012**, *85*, 1.
- [9] N. D. Hien, C. V. Nguyen, N. N. Hieu, S. S. Kubakaddi, C. A. Duque, M. E. Mora-Ramos, L. Dinh, T. N. Bich, H. V. Phuc, *Phys. Rev. B* **2020**, *101*, 1.
- [10] Q. H. Wang, K. Kalantar-Zadeh, A. Kis, J. N. Coleman, M. S. Strano, *Nat. Nanotechnol.* **2012**, *7*, 699.
- [11] C. H. Ho, Y. S. Huang, K. K. Tiong, *J. Alloys Compd.* **2001**, *317–318*, 222.
- [12] X.-G. Gao, X.-K. Li, W. Xin, X.-D. Chen, Z.-B. Liu, J.-G. Tian, *Nanophotonics* **2020**, *9*, 1717.
- [13] A. Varghese, D. Saha, K. Thakar, V. Jindal, S. Ghosh, N. V. Medhekar, S. Ghosh, S. Lodha, *Nano Lett.* **2020**, *20*, 1707.
- [14] F. Lai, N. Chen, X. Ye, G. He, W. Zong, K. B. Holt, B. Pan, I. P. Parkin, T. Liu, R. Chen, *Adv. Funct. Mater.* **2020**, *30*, 1.
- [15] T. Fujita, Y. Ito, Y. Tan, H. Yamaguchi, D. Hojo, A. Hirata, D. Voiry, M. Chhowalla, M. Chen, *Nanoscale* **2014**, *6*, 12458.
- [16] Y. C. Lin, H. P. Komsa, C. H. Yeh, T. Björkman, Z. Y. Liang, C. H. Ho, Y. S. Huang, P. W. Chiu, A. V. Krasheninnikov, K. Suenaga, *ACS Nano* **2015**, *9*, 11249.
- [17] O. B. Aslan, D. A. Chenet, A. M. van der Zande, J. C. Hone, T. F. Heinz, *ACS Photonics* **2016**, *3*, 96.
- [18] F. Liu, S. Zheng, X. He, A. Chaturvedi, J. He, W. L. Chow, T. R. Mion, X. Wang, J. Zhou, Q. Fu, H. J. Fan, B. K. Tay, L. Song, R. H. He, C. Kloc, P. M. Ajayan, Z. Liu, *Adv. Funct. Mater.* **2016**, *26*, 1169.
- [19] Z. G. Yu, Y. Cai, Y. W. Zhang, *Sci. Rep.* **2015**, *5*, 1.
- [20] D. Ghoshal, A. Yoshimura, T. Gupta, A. House, S. Basu, Y. Chen, T. Wang, Y. Yang, W. Shou, J. A. Hachtel, J. C. Idrobo, T. M. Lu, S. Basuray, V. Meunier, S. F. Shi, N. Koratkar, *Adv. Funct. Mater.* **2018**, *28*, 1.
- [21] X. Su, B. Zhang, Y. Wang, G. He, G. Li, N. Lin, K. Yang, J. He, S. Liu, *Photonics Res.* **2018**, *6*, 498.
- [22] K. Dileep, R. Sahu, S. Sarkar, S. C. Peter, R. Datta, *J. Appl. Phys.* **2016**, *119*, 114309.
- [23] Q. Sun, B. Zhang, L. Diao, B. Chen, K. Song, L. Ma, L. Ma, F. He, F. He, *J. Mater. Chem. A* **2020**, *8*, 11607.
- [24] K. Ghosh, S. Ng, C. Iffelsberger, M. Pumera, *ACS Appl. Energy Mater.* **2020**, *3*, 10261.
- [25] P. Pazhamalai, K. Krishnamoorthy, V. K. Mariappan, A. Sathyaseelan, S. J. Kim, *Mater. Chem. Front.* **2020**, *4*, 3290.
- [26] S. Kim, H. K. Yu, S. Yoon, N.-S. Lee, M. H. Kim, *CrystEngComm.* **2017**, *19*, 5341.
- [27] B. Jariwala, D. Voiry, A. Jindal, B. A. Chalke, R. Bapat, A. Thamizhavel, M. Chhowalla, M. Deshmukh, A. Bhattacharya, *Chem. Mater.* **2016**, *28*, 3352.
- [28] D. Hou, Y. Ma, J. Du, J. Yan, C. Ji, H. Zhu, *J. Phys. Chem. Solids* **2010**, *71*, 1571.
- [29] M. Rahman, K. Davey, S. Z. Qiao, *Adv. Funct. Mater.* **2017**, *27*, 1606129.
- [30] U. Res, C. M. Corbet, C. McClellan, A. Rai, S. S. Sonde, E. Tutuc, S. K. Banerjee, C. E. T. Al, *ACS Nano* **2015**, *9*, 363.
- [31] S. Cao, Y. Xing, J. Han, X. Luo, W. Lv, W. Lv, B. Zhang, Z. Zeng, *Nanoscale* **2018**, *10*, 16805.
- [32] M. Hafeez, L. Gan, H. Li, Y. Ma, T. Zhai, *Adv. Funct. Mater.* **2016**, *26*, 4551.
- [33] M. Heydari, M. Rahman, R. Gupta, *Int. J. Chem. Eng.* **2015**, *2015*, 481739.
- [34] S. Patel, S. H. Chaki, P. C. Vinodkumar, *Thermochim. Acta* **2020**, *689*, 178614.
- [35] R. M. Kannaujiya, A. J. Khimani, S. H. Chaki, S. M. Chauhan, A. B. Hirpara, M. P. Deshpande, *Eur. Phys. J. Plus.* **2020**, *135*, 1.